Technical University of Denmark

DTU

LiDAR observations of offshore winds at future wind turbine operating heights

Pena Diaz, Alfredo; Gryning, Sven-Erik; Hasager, Charlotte Bay

DTU Library
Technical Information Center of Denmark

LiDAR observations of offshore winds at future wind turbine operating heights

Alfredo Peña[1*], Sven-Erik Gryning[1], Charlotte B. Hasager[1]
[1]Wind Energy Department, Risø National Laboratory - DTU, DK-4000, Denmark
*alfredo.pena.diaz@risoe.dk

Abstract:

Combined LiDAR/cup anemometer observations performed in the summer of 2006 of wind speed profiles up to 161 m have been analyzed within an open sea sector at the Horns Rev offshore wind farm. The influence of atmospheric stability on the surface layer wind shear is studied by using a bulk formulation of the Richardson number to derive the Obukhov length from 10 minutes mean temperature and wind speed measurements. The influence of the boundary layer height on the wind speed profile gives a strong over-prediction of the wind speed in stable atmospheric conditions. A length scale model is suggested where the boundary layer height is taken into account. The resulting wind profile agrees well compared to the combined LiDAR/mast profiles in and beyond surface layer.

Keywords: Charnock, LiDAR, Marine boundary layer, Offshore, Surface layer, Wind profile.

1   Introduction

There is, without any doubt, an urgent need to study the wind resource over the sea due to the progress and planning of offshore wind farms in the coming years. In contrast with the situation over land, the knowledge of the wind and the turbulence characteristics in the MABL (Marine Atmospheric Boundary Layer) is still immature. From the theory and observations performed usually near coastal areas, e.g. in [1], [2], [3], [4] and [5], it is known that the wind speed is, in general, higher and the turbulence levels lower than over land due mainly to the small sea surface roughness. These conditions are attractive to the wind turbine manufacturers and wind farm developers, although the offshore environment represents other challenges which are as significant as the accurate measurement of wind speed like effective costs, wave loads, environmental impact, etc.

In the practical sense, the offshore wind resource must be studied in order to cover the whole range of heights where the cost-effective large wind turbines operate. Therefore, we are encouraged to develop techniques which can observe winds at heights beyond the SL (Surface Layer: the first 10% of the atmospheric boundary layer) where most of the measurements and modeling has been done. Ground-based remote sensing instruments have been improved in the last years to observe accurately the wind speed as shown by [6] over land and [7] and [2] over sea. In particular, LiDAR (Light Detection And Ranging) has shown good results at offshore platforms and agrees well with measurements from cup anemometers [8], [2].

In this paper, we analyze observations of the wind speed profile performed with a LiDAR at the platform of the Horns Rev offshore wind farm in combination with cup anemometers from a meteorological mast in the surrounding area. The observations are combined resulting in an extended wind speed profile which reaches heights up to 161 m AMSL (Above Mean Sea Level). We present a model for the wind profile which takes into account the effects of atmospheric stability and the BL (Boundary Layer) height which have a strong influence on the wind speed behavior already at heights around 45 m AMSL in stable atmospheric conditions. This is achieved following closely the corrections of the "traditional" surface layer wind profile over land given in [9].

2 Theory

2.1 The extended wind profile

For homogeneous and stationary flow, [10] described the variation of mean wind speed with height as:

$$\frac{\partial u}{\partial z} = \frac{u_*}{\ell} \qquad (1)$$

where u is the mean wind speed, z the height above ground, u_* the friction velocity and ℓ is the mixing length scale. Here, u_* is modeled to account for the decrease with height following [9]:

$$u_* = u_{*o}\left(1 - \frac{z}{z_i}\right) \qquad (2)$$

where u_{*o} is the friction velocity close to the ground and z_i is the BL height. ℓ is modeled by inverse summation (following the analysis of [9]) of two length scales:

$$\frac{1}{\ell} = \frac{\phi_m}{\ell_{SL}} + \frac{1}{\ell_{BSL}} \qquad (3)$$

where ℓ_{SL} is the length scale in the SL (it is assumed to be proportional to height, $\ell_{SL} = \kappa z$), ℓ_{BSL} is the length scale beyond surface layer and κ is the von Karman constant ($\approx$0.4). The last is modeled to decrease linearly with height until it reaches the BL height, $\ell_{BSL} = \kappa(z_i - z)$. ϕ_m is the so-called dimensionless wind shear defined as:

$$\phi_m = \frac{\kappa z}{u_{*o}} \frac{\partial u}{\partial z}. \qquad (4)$$

Eq. (3) implies that MOST (Monin-Obukhov similarity theory) will correct ℓ near the ground to account for the effect of atmospheric stability using the ϕ_m function. Several authors, e.g. [11], [12], [13], [14] and [15] have studied the variation of ϕ_m with stability and found the following relations depending on the atmospheric condition: unstable, neutral and stable, respectively:

$$\phi_m = \left(1 - a\frac{z}{L}\right)^p \qquad (5)$$

$$\phi_m = 1 \qquad (6)$$

$$\phi_m = \left(1 + b\frac{z}{L}\right) \qquad (7)$$

where [11] found the values a=15, b=4.7 and p=-1/4 and [14] a=16 and p=-1/3 for the unstable correction. L is the Obukhov length which relates the production of momentum and heat flux (the estimation of L is performed in Section 2.3).

In Figure 1 is illustrated the behavior of ℓ with height in neutral atmospheric conditions (i.e. ϕ_m=1) for two combinations of length scales.
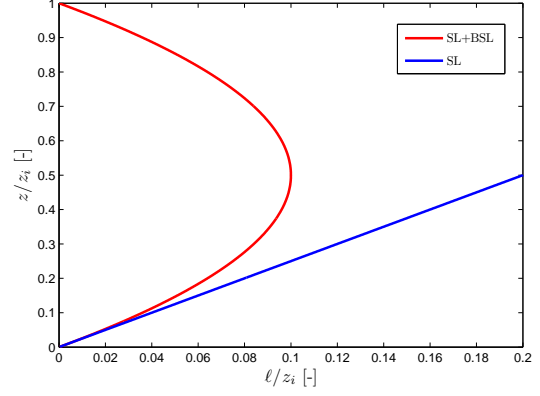

Figure 1: Length scale variation in the neutral atmosphere. SL: $\ell = \ell_{SL} = \kappa z$. SL+BSL: Using Eq. (3).

The blue line in Figure 1 is obtained with ℓ proportional to z as it is traditionally assumed in SL scaling (see [16]). In the SL ($z/z_i \leq 0.1$), both blue and red curves show the same behavior within this layer but the growth of the length scale is controlled with Eq. (3) beyond SL.

Introducing Eq. (3) and (2) into (1) and integrating with height, the result, for the unstable, neutral and stable wind profile, respectively, is:

$$u = \frac{u_{*o}}{k}\left[\ln\left(\frac{z}{z_o}\right) - \psi_m\left(\frac{z}{L}\right)\right] \qquad (8)$$

$$u = \frac{u_{*o}}{k}\ln\left(\frac{z}{z_o}\right) \qquad (9)$$

$$u = \frac{u_{*o}}{k}\left[\ln\left(\frac{z}{z_o}\right) - \psi_m\left(\frac{z}{L}\right)\left(1 - \frac{z}{2z_i}\right)\right] \qquad (10)$$

where z_o is the aerodynamic roughness length and ψ_m is the so-called universal stability function which depends on the form of the ϕ_m function (see Appendix A). It is interesting to note that Eq. (8) and (9) give the same result as the traditional surface layer wind profile for unstable and neutral atmospheres. For measurements up to 160 m, the effect of the BL height can be observed only in the stable wind profile

2.2 The sea roughness length

The roughness length depends on the wind speed over the sea. This dependence has been commonly modeled using the Charnock's relation [17]:

$$z_o = \alpha_c\frac{u_{*o}^2}{g} \qquad (11)$$

where α_c is the Charnock's parameter, with typical values in the range 0.01-0.06, and g is the gravitational acceleration. Many studies, e.g. [18] and [19], showed that α_c in Eq. (11) depends on different parameters such as wave age and fetch. Here, it is assumed to be constant with a value α_c=0.012 which was found to describe well the mean wind speed profile from measurements performed at Horns Rev in [20] and [2].

2.3 Atmospheric stability

The state of the atmosphere is estimated using the method applied in [21] where the bulk Richardson number is used:

$$Ri_b = -\frac{gz\Delta\Theta_{s/z}}{T_z u_z{}^2}. \qquad (12)$$

$\Delta\Theta_{s/z}$ in Eq. (12) corresponds to the mean potential temperature difference between the SST (Sea Surface Temperature) and the reference height z, where mean Temperature T_z and mean wind speed u_z are also measured. The dimensionless stability parameter, z/L in Eq. (5) and (7), is related with Ri_b depending on the condition of the atmosphere ($Ri_b < 0$ for unstable and $Ri_b > 0$ for stable atmospheres, respectively):

$$\frac{z}{L} = C_1 Ri_b \qquad Ri_b < 0 \qquad (13)$$

$$\frac{z}{L} = \frac{C_2 Ri_b}{1 - C_3 Ri_b} \qquad Ri_b > 0 \qquad (14)$$

where C_1, C_2 and C_3 are constant values.

3 The experiment

The experiment combines wind speed measurements observed at two locations in the periphery of the Horns Rev offshore wind farm. The wind farm is located at the west coast of Denmark in the North Sea (see Figure 2) and consists of 80 Vestas V80 turbines installed in a oblique rectangle. At the North-west part of this rectangle, a meteorological mast (M2) is installed at around 18 km from the nearest coast line. On M2, wind speeds are observed at 15, 30, 45 and 62 m AMSL (Above Mean Sea Level) using Risø cup anemometers (at the first three heights, the instruments are side-mounted on 2 m booms, whereas at the 62 m AMSL height the instrument is top-mounted). Wind vanes at 43 and 60 m AMSL and temperature sensors at 55, 13 m AMSL and 4 BMSL (Below Mean Sea Level) are

also installed on M2. Further information about the mast instrumentation and flow distortion effects due to the mast is available in [20], [2] and [22].

During the months of May to October 2006, a commercial ZephIR wind LiDAR unit from QinetiQ was installed on the transformer/platform of the wind farm which is about 5.5 km east from M2. The LiDAR was placed at 20 m AMSL scanning conically the atmosphere at an angle of 30.6° to the zenith. Observed wind speeds at heights 63, 91, 121 and 161 AMSL are used in this study. The LiDAR measures the line-of-sight velocity, V_{LOS}, which can be decomposed into the three wind speed components (u, v and w) given several azimuth directions (see Figure 3). A more detailed description of the instrument and the campaign is given in [2] and [20]. In [2] it is also described a simple methodology used to avoid contamination of the wind speed measurements due to clouds using an observation at 300 m AMSL height and in [20] the effect of the increasing vertical effective measuring volume on the measurements is studied (also illustrated in Figure 3).
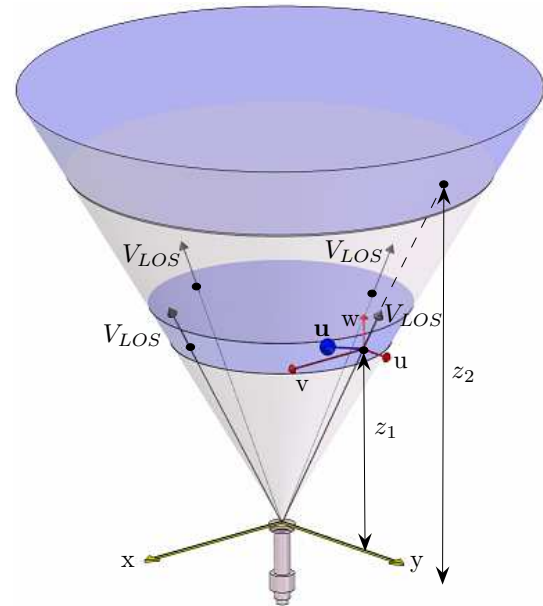

Figure 3: LiDAR scanning configuration.

For the analysis, only wind speeds above 3 ms^{-1} are considered at the 15 m AMSL height. The wind directions are selected on the overlapping M2/platform sector which corresponds to an open sea sector. This results in the directions $\theta_{P/M2} \geq 270° \vee \theta_{P/M2} \geq 10°$. Both LiDAR and M2 observations are stored as 10 min (minutes)
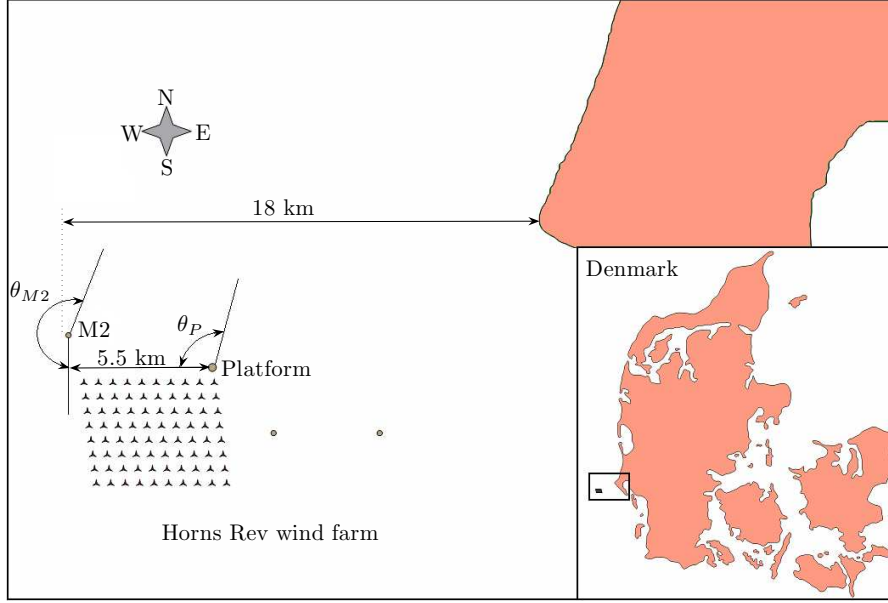
Figure 2: Horns Rev wind farm in the Danish North Sea.

averages.

4 Results

4.1 Wind shear variation with atmospheric stability

The effect of atmospheric stability on the wind profile is analyzed using the ϕ_m function in Eq. (4). The variation of ϕ_m with z/L from the observations can then be compared with the relations given in Eq. (5), (6) and (7), e.g. using the values $a = 12$, p=-1/3 and b=4.7. The derivation of ϕ_m by using Eq. (4) involves the calculation of the wind speed gradient $\partial u/\partial z$. Following [13] this is determined by fitting the wind speed observations at 15, 30 and 45 m AMSL to a second-order polynomial in $\ln(z)$:

$$u = u_o + A \ln(z) + B \ln(z)^2 \qquad (15)$$

where u_o, A and B are computed using a least-squares method. Eq. (15) is differentiated with height:

$$\frac{\partial u}{\partial z} = \frac{A + 2B \ln(z)}{z} \qquad (16)$$

and the result is introduced into Eq. (4) which gives:

$$\phi_m = \frac{\kappa}{u_{*o}} \left(A + 2B \ln(z) \right). \qquad (17)$$

z in Eq. (17) is here referenced to a mean logarithmic height, z_p:

$$z_p = \frac{45 - 15}{\ln(45/15)} \qquad (18)$$

and thus, the variation of ϕ_m with stability should now be analyzed using the ratio z_p/L.

For the estimation of L, we applied the bulk Richardson method given in Eq. (13) and (14) using the values 10, 15 and 5 for the constants C_1, C_2 and C_3, respectively. Ri_b in Eq. (12) is estimated from the measurements of air and water mean temperatures at 13 m AMSL and 4 m BMSL, and mean wind speed at 15 m AMSL.

The last parameter required for the estimation of ϕ_m is u_{*o} which is computed by a least-squares method using Charnock's relation combined with the traditional surface layer wind profile for the 15 m wind speed observation (the so-called Charnock's profile derived friction velocity):

$$u_{15} = \frac{u_{*o}}{k} \left[\ln \left(\frac{15}{\alpha_c \frac{u_{*o}^2}{g}} \right) - \psi_m \left(\frac{15}{L} \right) \right]. \qquad (19)$$

In Figure 4 is illustrated the comparison between the variation of ϕ_m with z_p/L registered from the measurements and the predicted values of MOST using Eq. (5) and (7).

The differences between the locally weighted and the predicted curve are relatively small on the whole range of analysis which corresponds
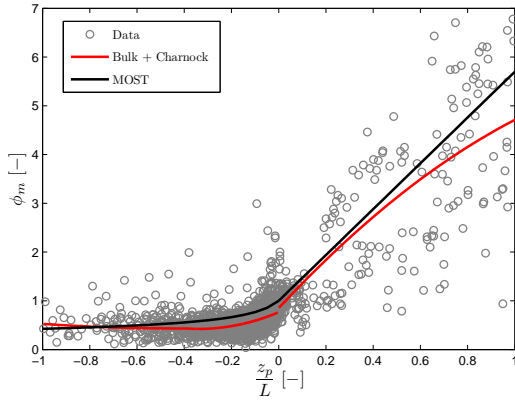
Figure 4: Variation of dimensionless wind shear with dimensionless stability parameter. The bulk method is combined with Charnock's friction velocity for the measurements. The red line corresponds to a locally weighted curve computed from the scatter data using a least-squares polynomial fitting.

to $-1 \leq z_p/L \leq 1$, i.e. to $|L| \geq 27$ where MOST can be applied to surface layer scaling. The differences are bigger in the near neutral/unstable side ($-0.4 \leq z_p/L \leq 0$) where the measurements show more steep profiles (the wind speed varies little with height) as well as in the very stable side compared to the stability correction in Eq. (7).

4.2 Wind profiles

For the analysis of the mean wind speed profiles, the 10 min individual wind profiles are classified in atmospheric stability classes according to intervals of L. In each class, several mean parameters are computed and the results are given in Table 1.

The different atmospheric stability classes were suggested in [9] from the analysis of wind profiles over flat and homogeneous terrain. From Table 1, it is interesting to note that the observations correspond to a quite unstable period where u_{*o} increases the closer the atmospheric conditions are to neutral. In the very stable class, the number of measured profiles increases and the value of $\overline{L}$ is relatively low; therefore, it is expected to observe a high variation of mean wind speed with height in this class.

The mean wind speed profile is computed in each atmospheric stability class combining the observations of both LiDAR and M2. The comparison between the observations and the pre-

dicted wind profile using the traditional surface layer wind profile (Eq. (19) but for the whole range of z) is illustrated in Figure 5 where the three first observations (15, 30 and 45 m AMSL) correspond to the cup anemometers and the last four to the LiDAR measurements (63, 91, 121 and 161 m AMSL).
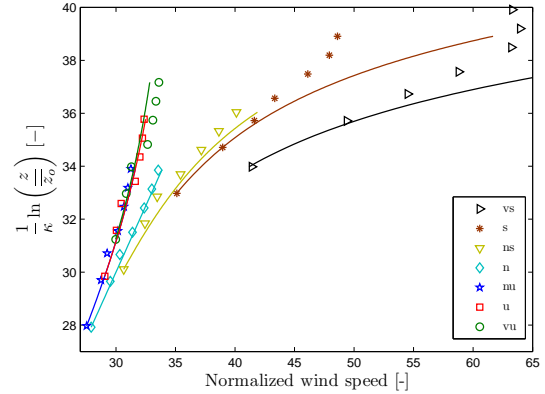

Figure 5: Mean wind speed profiles in each stability class. The solid lines represent the prediction using the traditional surface layer scaling of the wind profile. The markers the observations in the different stability classes.

In Figure 5, the height in the y-axis is normalized with the mean roughness length, $\overline{z_o}$, in each stability class which is computed using Charnock's relation and the values of $\overline{u_{*o}}$ given in Table 1. This normalization displaces the level of the profiles in the y-axis and is used to show the different values of $\overline{z_o}$ which actually decreases the farther the measurements are from neutral conditions [3].

In general, the LiDAR observations extend well the mast profiles for all atmospheric conditions. The largest differences between the predicted values and the observations are found in the stable classes where the traditional surface layer profile over-predicts the wind speed already at a height of 45 m AMSL. This is likely due to the influence of the BL height which for practical purposes can be approximated as:

$$z_i = \frac{1}{10} \frac{\overline{u_{*o}}}{f_c} \qquad (20)$$

where f_c is the Coriolis parameter. For the two most stable atmospheric classes (s and vs), Eq. (20) gives values of 126 and 103 m AMSL for z_i, respectively, i.e. the BL height is within the range of measurements. The expression in Eq. (10) is then used to correct the prediction curves

Table 1: Wind profile mean parameters in each stability class.

Atmospheric stability class	Obukhov length interval	$\overline{L}$ [m]	$\overline{u_{*o}}$ [ms^{-1}]	No. of Profiles
Very stable (vs)	$10 \leq L \leq 50$	24	0.12	120
Stable (s)	$50 \leq L \leq 200$	83	0.15	64
Neutral/stable (ns)	$200 \leq L \leq 500$	324	0.27	36
Neutral (n)	$-500 \geq L \geq 500$	-1207	0.42	318
Neutral/unstable (nu)	$-500 \leq L \leq -200$	-294	0.41	652
Unstable (u)	$-200 \leq L \leq -100$	-139	0.28	552
Very unstable (vu)	$-100 \leq L \leq -50$	-72	0.21	306

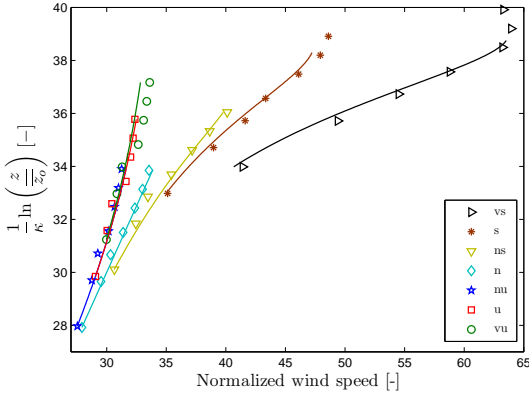on the stable atmospheric wind profiles and the result is illustrated in Figure 6.

Figure 6: Mean wind speed profiles in each stability class. The solid lines represent the prediction using Eq. (8), (9) and (10). The markers the observations in the different stability classes.

As Figure 6 shows, the correction added to the traditional stable wind profile due to the proximity of the BL height in Eq. (10) is in agreement with the observations and can be used until the BL height is reached. The traditional wind profile predicts an increasing wind speed with height due to the infinite increasing length scale $\ell = \kappa z$. The length scale model given in Eq. (3) limits this infinite growing mixing length and, thus, the wind speed.

5 Conclusions

The offshore wind speed profile has been successfully measured with combined LiDAR/mast data and modeled up to heights about 160 m AMSL. By using MOST in combination with the traditional surface layer wind profile commonly used over land, the predicted profile shows good agreement under unstable and neutral conditions but over-predicts the wind speed in the stable atmospheres beyond surface layer.

A model is proposed to account for the effect of the boundary layer height on the friction velocity and the mixing length scale. This effect vanishes in the unstable and neutral atmospheres but a correction is found for the stable wind profile. The result of the correction is in agreement with the combined LiDAR/mast observations up to the height where the boundary layer height is reached.

A bulk Richardson number method combined with Charnock's relation is used to derive the behavior of the variation of the wind shear with atmospheric stability. The variation registered from the observations in the surface layer show good agreement with the commonly used expressions in the literature [14] and [15].

Finally, it must be noticed that the measurements correspond to an open sea sector where the land and wind farm wake effects are minimum. In this study it is assumed that the atmospheric stability observed in the profiles measured at the platform, where the LiDAR was installed, is close to the stability found at the mast location. On this open sea sector, high correlations (near unity) for the mean wind speed where already found by [20] and [2], when the LiDAR was compared against cup anemometers from masts in the vicinity of the wind farm.

Acknowledgments

Appendix A

The ψ_m function is equal to zero for neutral atmospheres. For stable and unstable atmospheres, respectively, the expressions can be found in [11] and [15]:

$$\psi_m \left(\frac{z}{L} \right) = -b\frac{z}{L} \qquad (21)$$

$$\psi_m \left(\frac{z}{L} \right) = \frac{3}{2} \ln \left(\frac{1 + y + y^2}{3} \right) - \sqrt{3} \arctan \left(\frac{2y + 1}{\sqrt{3}} \right) + \frac{\pi}{\sqrt{3}} \qquad (22)$$

where $y = \left(1 - a\frac{z}{L} \right)^{-p}$ and p=-1/3.

References

[1] Högström U, Smedman AS, Bergström H. Calculation of wind speed variation with height over the sea. Wind Engineering 2006; **30**:269–286.

[2] Peña A, Hasager C, Gryning SE, Courtney M, Antoniou I, Mikkelsen T. Offshore wind profiling using LiDAR measurements. Submitted to Wind Energy 2007; .

[3] Peña A, Gryning SE. Charnock's roughness model and non-dimensional profiles over the sea. Submitted to Boundary-Layer Meteorology 2007; .

[4] Barthelmie R, Hansen O, Enevoldsen K, Højstrup J, Frandsen S, Pryor S, Larsen S, Motta M, Sanderhoff P. Ten years of meteorological measurments for offshore wind farms. J. Sol. Energy Eng. 2005; **127**(2):170–176.

[5] Tambke J, Lange M, Focken U, Wolff JO, John A, Bye T. Forecasting offshore wind speeds above the North Sea. Wind Energ. 2005; **8**:3–16.

[6] Smith D, Harris M, Coffey A, Mikkelsen T, Jørgensen H, Mann J, Danielian R. Wind lidar evaluation at the danish wind test site in Høvsøre. Wind Energ. 2006; **9**:87–93.

[7] Antoniou I, Jørgensen H, Mikkelsen T, Frandsen S, Barthelmie R, Perstrup C, Hurtig M. Offshore wind profile measurements from remote sensing instruments. In: Proceedings of the European Wind Energy Association Conference & Exhibition. Athens, 2006; .

[8] Kindler D, Oldroyd A, MacAskill A, Finch D. Offshore-erprobung eines LiDAR-windmesssystems auf FINO-1. In: Proceedings of the Conference on Offshore Wind Energy. Hamburg, 2006; .

[9] Gryning SE, Batchvarova E, Brümmer B, Jørgensen H, Larsen S. On the extension of the wind profile over homogeneous terrain beyond the surface layer. Boundary-Layer Meteorol. 2007; **124**:251–268.

[10] Panofsky H. Tower Micrometeorogy. In: Haugeb DA (ed) Workshop on Micrometeorolgy. American Meteorology Society, pp 151-176, 1973.

[11] Businger J, Wyngaard J, Izumi Y, Bradley E. Flux-profile relationships in the atmospheric surface layer. J. Atmos. Sci. 1971; **28**:181–189.

[12] Dyer A. A review of flux-profile relatioships. Boundary-Layer Meteorol. 1974; **7**:363–372.

[13] Högström U. Non-dimensional wind and temperature profiles in the atmospheric surface layer: a re-evaluation. Boundary-Layer Meteorol. 1988; **42**:55–78.

[14] Carl D, Tarbell T, Panofsky H. Profiles of wind and temperature from towers over homogeneous terrain. J. Atmos. Sci. 1973; **30**:788–794.

[15] Grachev A, Fairall C, Bradley E. Convective profile constraints revisited. Boundary Layer-Meteorol. 2000; **94**:495–515.

[16] Panofsky H, Dutton J. Atmospheric turbulence. John Wiley & Sons, 1984.

[17] Charnock H. Wind stress over a water surface. Q. J. R. Meteorol. Soc. 1955; **81**:639–640.

[18] Lange B, Larsen S, Højstrup J, Barthelmie R. Importance of thermal effects and the sea surface roughness for offshore wind resource assessment. J. Wind Eng. Ind. Aerodyn. 2004; **92**:959–988.

[19] Lange B, Larsen S, Højstrup J, Barthelmie R. The influence of thermal effects on the wind speed profile of the coastal marine boundary layer. Boundary-Layer Meteorol. 2004; **112**:587–617.

[20] Hasager C, Peña A, Mikkelsen T, Court-ney M, Antoniou I, Gryning SE, Hansen P, Sørensen P. 12 MW Horns Rev experiment. Technical Report Risoe-R-1506(EN), Risø National Laboratory, Roskilde, URL:www.risoe.dk, 2007.

[21] Grachev A, Fairall C. Dependence of the Monin-Obukhov stability parameter on the bulk Richardson number over the ocean. J. of Applied Meteorol. 1996; **36**:406–414.

[22] Elsam Engineering. Wake effect east of the Horns Rev offshore wind farm. Technical Report 209918, Elkraft System, PSO - F&U 2002/FU2103, Eltra no. 4158, ELSAM-VU111, Fredericia, 2005.